Perturbation of the Stability of Amyloid Fibrils through Alteration of Electrostatic Interactions

Sarah L. Shammas,[†]* Tuomas P. J. Knowles,[†] Andrew J. Baldwin,[†] Cait E. MacPhee,[‡] Mark E. Welland,[§] Christopher M. Dobson,[†] and Glyn L. Devlin[¶]

[†]Department of Chemistry, University of Cambridge, Cambridge, United Kingdom; [‡]School of Physics, University of Edinburgh, Edinburgh, United Kingdom; [§]Nanoscience Centre, University of Cambridge, Cambridge, United Kingdom; and [¶]Department of Biochemistry and Molecular Biology, Monash University, Clayton, Victoria, Australia

ABSTRACT   The self-assembly of proteins and peptides into polymeric amyloid fibrils is a process that has important implications ranging from the understanding of protein misfolding disorders to the discovery of novel nanobiomaterials. In this study, we probe the stability of fibrils prepared at pH 2.0 and composed of the protein insulin by manipulating electrostatic interactions within the fibril architecture. We demonstrate that strong electrostatic repulsion is sufficient to disrupt the hydrogen-bonded, cross-β network that links insulin molecules and ultimately results in fibril dissociation. The extent of this dissociation correlates well with predictions for colloidal models considering the net global charge of the polypeptide chain, although the kinetics of the process is regulated by the charge state of a single amino acid. We found the fibrils to be maximally stable under their formation conditions. Partial disruption of the cross-β network under conditions where the fibrils remain intact leads to a reduction in their stability. Together, these results support the contention that a major determinant of amyloid stability stems from the interactions in the structured core, and show how the control of electrostatic interactions can be used to characterize the factors that modulate fibril stability.

INTRODUCTION

Amyloid fibrils are filamentous, β-sheet-rich protein superstructures with typical diameters of ~10 nm and lengths of the order of microns. In vivo, these structures can form as a result of aberrant misfolding and subsequent aggregation of normally soluble proteins, leading to their accumulation in various organs and tissues of the body, processes that are associated with more than 40 clinical disorders, including Alzheimer's disease and type II diabetes (1). In other cases, however, controlled formation of amyloid structures is connected to important biological functionality such as the catalytic production of melanin (2) and the formation of functional coating materials (3). In addition, amyloid fibrils with structural characteristics in common with those formed in vivo can also be formed in vitro from many different unrelated peptides and proteins (4). This finding, in addition to the observations that amyloidogenic proteins can be remarkably variable in both sequence and native structure, has led to the suggestion that fibril formation represents a common or generic property of polypeptide chains (1) driven by common intermolecular interactions between the polypeptide main chains (5).

Structural studies on amyloid fibrils have revealed that they share a common cross-β structural motif, in which individual β-strands lie perpendicular to the fibril axis with the resultant β-sheets stacked in the parallel direction to produce protofilaments (6,7). In many cases, these protofilaments associate laterally to generate hierarchical structures.

Amyloid fibrils typically demonstrate remarkable stability and their extreme resistance to high hydrostatic pressures and temperatures has been used to support the suggestion that the amyloid structure, under some conditions, can represent a lower free energy state than that of the native fold of proteins (8,9). The stability of these structures is of great importance from a biomedical perspective, as this characteristic is likely to impede their disaggregation and clearance in vivo. This property could, however, also underlie the benefits associated with exploitation of amyloid fibrils for functional purposes in nature (10) as well as providing inspiration for the design and implementation of novel nanomaterials based on protein nanostructures (5,11).

The molecular origin of fibril stability has recently been the focus of intense investigation, and the characteristic main-chain hydrogen bonding between the constituent polypeptides has been identified as an important contribution (5,12,13). Recent high-resolution structural studies of amyloid structures have also identified additional sources of fibril stability; these include intermolecular hydrogen bonding, ionic pairing, and aromatic π-π interactions between amino-acid side chains (7,12,14). In addition, the entropic energy resulting from the release of structured solvent molecules in the densely packed core (13,15) of amyloid fibrils is likely to be a significant factor in enhancing their stability.

In this article, we examine the contribution of electrostatic interactions to the stability of fibrils composed of the protein insulin, and use the active control of such interactions to probe the magnitude and nature of the stability of the amyloid structure. Insulin is a small, α-helical protein

comprising two disulfide cross-linked polypeptide chains (A and B), which readily forms amyloid fibrils under acidic conditions (16). It has been established for many years that insulin fibrils produced in this way dissociate under alkaline conditions (17,18). Here, we examined the mechanism of this dissociation process by preparing fibrils at pH 2.0 and measuring their stability as a function of the pH of the solution in which the fibrils are subsequently immersed. The results show that the stability of insulin fibrils is sensitive to the net charge on the polypeptide chains, and the disruption of ion-pairings. Furthermore, by combining this approach with chemical denaturation, we observe a correlation between fibril stability and β-sheet content, suggesting that, at least in this case, the origin of fibril stability stems from the interactions within the hydrogen-bonded cross-β structural motif common to amyloid fibrils.

MATERIALS AND METHODS

Preparation of insulin fibrils

Insulin fibrils were prepared in seeded reactions to produce a homogeneous fibril suspension with minimal chemical degradation and very few higher order aggregates such as spherulites (as determined by cross-polarized light microscopy) (19,20). A single round of seeding using 2.5–5% w/w preformed fibrils was sufficient to produce a homogeneous fibril suspension. Seed fibrils were prepared by incubation of bovine insulin at 10 mg/ml in dilute HCl at pH 2.0 and 60°C for 16 h. The seeded solutions were incubated at 60°C until a thick gel formed (16).

pH dependence of the extent of insulin fibril dissociation

Aliquots of insulin fibrils in dilute HCl at pH 2.0 were added into buffered solutions as follows: glycine in the pH ranges 2.0–3.5 (I: ~10–30 mM) and 9.5–10.5 (I: ~10–30 mM); acetate, pH 4.0–5.5 (I: ~10–30 mM); citrate, pH 6.0–7.0 (I: ~10–30 mM); Tris-HCl, pH 7.5–9.0 (I: ~30–10 mM); and phosphate, pH 11.0–12.5 (I: ~60–150 mM) such that the final protein and buffer concentrations were 0.3 mg/ml and 30 mM, respectively. Over the range where significant dissociation was observed, the ionic strength varied from ~10 mM to 60 mM. However, similar results were obtained when the pH of a separate fibril stock solution was adjusted with NaOH, where the ionic strength varied from only 10 mM at pH 2 to 11 mM at pH 11 (data not shown).

The solutions were incubated at room temperature for 48 h, and the extent of fibril dissociation measured by sedimenting the fibrils in an Optima TLX ultracentrifuge (Beckman-Coulter, Fullerton, CA) at ~288,000 $\times$ g for 40 min. The supernatants were subsequently neutralized via the addition of concentrated Tris-HCl (pH 7.5) and the absorbance measured at 280 nm to calculate the protein concentration using an extinction coefficient of 6335 M^{-1} cm^{-1} (www.expasy.org).

Kinetics of insulin fibril dissociation

Insulin fibrils were diluted to a final concentration of 0.2 mg/ml in dilute HCl at pH 2.0. Dissociation was initiated by the addition of small volumes of concentrated NaOH and monitored by the change in solution turbidity at 360 nm using a model No. 400 Scan UV-visible spectrophotometer (Varian, Cary, NC) with a Peltier temperature controller. The pH of each solution was measured at the conclusion of each reaction.

Transmission electron microscopy

Samples were deposited onto Formvar- and carbon-coated 400-mesh copper grids and negatively stained with uranyl acetate. Electron micrographs were acquired on a Tecnai 20 transmission electron microscope (TEM; Philips, Amsterdam, The Netherlands) at a voltage of 120 kV.

Fourier transform infrared spectroscopy and analysis

Labile hydrogens in bovine insulin were exchanged for deuterons by dissolving the protein to a final concentration of 5 mg/ml in D_2O at pH* 1.6 (the pH meter electrode reading in the deuterated solvent without correction for isotope effects). Solutions were incubated at 37°C for 16 h and subsequently lyophilized. Seeded fibrils were produced as outlined above, except that D_2O at pH* 1.6 was used as the solvent and the protein was incubated at a concentration of 20 mg/ml. Fibril solutions were adjusted to the desired pH* by the addition of NaOD. Spectra were recorded with an Equinox 55 Fourier transform infrared (FTIR) spectrometer (Bruker Optics, Billerica, MA). Samples were held between CaF_2 windows using a 50-μm Teflon spacer. For each spectrum, 256 interferograms were coadded at room temperature and at 2 cm^{-1} resolution, and the background absorption of D_2O was subtracted. Spectra between 1600 and 1700 cm^{-1} were normalized to unity, and the fitting of component peaks to Gaussian functions (21) was performed using the OriginPro 7.5 software package (OriginLab, Northampton, MA).

Guanidinium thiocyanate-induced fibril dissociation

Insulin fibrils were added at a final concentration of 0.3 mg/ml to solutions containing various concentrations of guanidinium thiocyanate and either 30 mM glycine (pH 2.0), acetate (pH 4.0), citrate (pH 6.0), or Tris-HCl (pH 8.0). Solutions were incubated at room temperature for 48 h, before centrifugation in an Optima TLX ultracentrifuge (Beckman-Coulter) at ~288,000 $\times$ g for 40 min. This incubation period was demonstrated to be sufficient for the samples to reach equilibrium (see Fig. S2 in the Supporting Material). The protein concentration of the supernatants was determined using the Bradford assay (22).

RESULTS AND DISCUSSION

Fibril stability is susceptible to electrostatic repulsion between constituent polypeptide chains

To determine the pH dependence of insulin fibril stability, solutions of fibrils produced at pH 2.0 were adjusted to a range of pH values between 2.0 and 12.5 and incubated at room temperature for 48 h. Determination of the soluble fraction of insulin in these solutions subsequent to ultracentrifugation showed no observable dissociation of the fibrils between pH 2.0 and 8.0 (Fig. 1, *left panel*). Between pH 8.0 and 11.0, however, increasing amounts of insulin were present in the supernatants indicating that dissociation had taken place in these solutions, consistent with recent findings of Malisauskas et al. (23) who demonstrated disaggregation of insulin amyloid fibrils (grown under similar conditions) in this pH range using Thioflavin T fluorescence as a probe.

This conclusion was confirmed by examination of the fibril solutions by TEM before centrifugation (Fig. 1, *right*
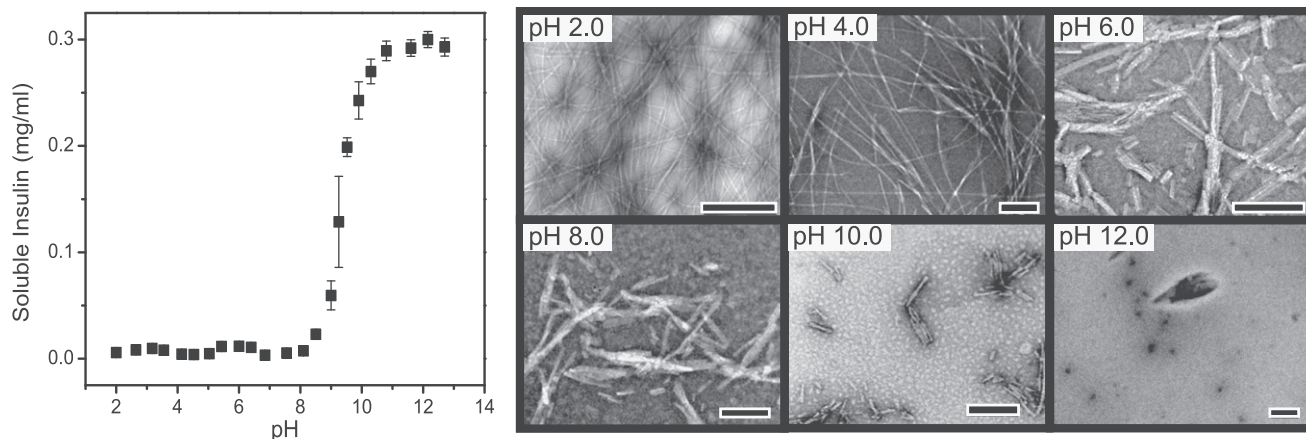
FIGURE 1 pH dependence of insulin fibril dissociation. (*Left panel*) The extent of fibril dissociation at steady state was determined by measuring the protein concentration of the supernatants from ultracentrifuged solutions of fibrils that had been incubated at various pH values for 48 h. (*Right panels*) Representative fibril TEM images are from samples at various pH values as indicated in the figure. Scale bars represent 200 nm.

panels). In agreement with the sedimentation data described above, abundant fibrils were observed between pH 2.0 and pH 8.0; fewer fibrils were present at pH 10.0, however, and none were detected at pH 12.0, confirming their dissociation in this pH range. Although no significant dissociation into soluble species occurred below pH 8.0, fibrils at pH 6.0 and 8.0 are morphologically distinct from those at pH 2.0 and 4.0, appearing shorter with a higher degree of lateral association.

The fibril dissociation reaction was found to have reached completion and to be reversible (see the Supporting Material), so the observed dissociation reflects a change in stability between the soluble and pH 2-like fibrillar forms of insulin. Soluble insulin has been shown to have complex self-association behavior, particularly in the presence of zinc and at neutral pH (24). However, because insulin oligomers become less stable as the pH is increased above neutral (25), the decrease in fibrillar material must be caused by destabilization of fibrils, rather than stabilization of the soluble form. Furthermore, it is expected that the majority of soluble insulin is monomeric over the pertinent pH range. This is because of the high concentration dependence of the insulin oligomer population (26–28) and the relatively low soluble insulin concentrations utilized in these studies (≤0.3 mg/ml). In addition, insulin oligomers dissociate from pH 7 to pH 9 (25) even at 2.5 mg/ml, whereas the majority of fibril dissociation is observed from pH 9.0 to pH 10.5.

To gain insight into the driving forces behind the dissociation reaction, we estimated the net charge Q on the insulin molecules as a function of pH based on the ionizable groups present in the insulin sequence (Fig. 2 *A*). An isoelectric focusing gel showed that native pH 10.0 bovine insulin incubated at room temperature for 48 h experienced no change in pI (data not shown), suggesting that in the soluble form at least, there is no significant deamidation of the asparagine or glutamine residues (to aspartic acid or glutamic acid,

respectively) within the timescale of the experiment. The pK_a values of the ionizable groups present in amyloid fibrils are likely to deviate from their intrinsic values due to the
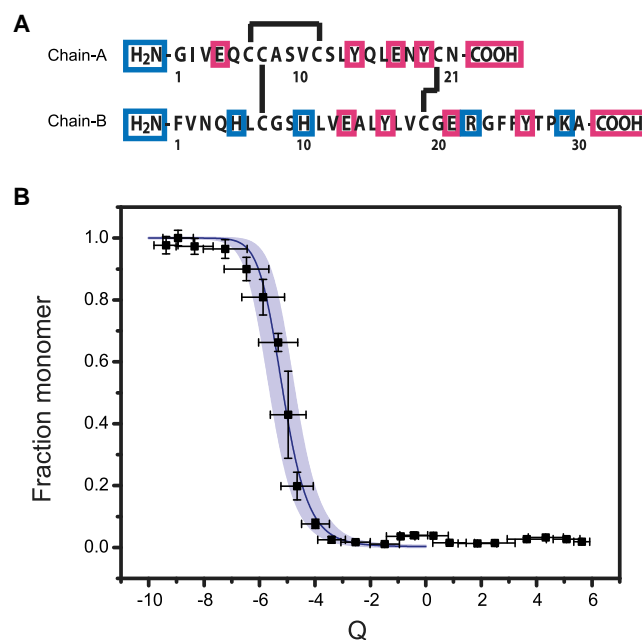

FIGURE 2 Dependence of insulin fibril dissociation on polypeptide net charge. (*A*) The amino-acid sequence of insulin is shown including the position of disulfide bonds (*black lines*). Residues with acidic and basic ionizable moieties are highlighted in magenta and blue, respectively. (*B*) The correlation between the predicted net charge (Q) of the insulin molecule and the fraction of soluble protein liberated from the fibrils in the pH range 2.0–12.5. Where $Q \leq 0$, the data were fitted to a linear polymerization model (34), modified such that the free energy difference between the soluble and fibrillar state has been split into an electrostatic component and a contribution to fibril stability in the absence of charge (see main text). Errors were assigned to each value of Q to account for the deviations of the pK_a values of ionizable moieties in the folded environment of the fibril, based on the variability of pK_a values observed for folded proteins (29). (*Shaded region overlaying the data*) Corresponding error in the line of best fit.

effects of the folded context of the fibril. Given the challenges associated with empirically determining these pK_a values for amyloid fibrils using conventional approaches such as solution-state NMR spectroscopy, we estimated Q by utilizing average pK_a values tabulated by Pace et al. (29) for some 541 ionizable moieties from 78 folded proteins (as described in the Supporting Material).

The fraction of soluble protein is shown as a function of the estimated polypeptide net charge in Fig. 2 B. Between pH 2.0 and 8.0, the range in which fibril dissociation is below detectable limits, the estimated net charge on the protein changes from 5.9 to -3.3, the isoelectric point being pH 5.5. Across the pH regime in which dissociation is readily detectable (pH 8.0–12.0), the estimated net charge increases from -3.3 to -9.2. We consider here that fibril stability is readily perturbed in this high pH regime, owing to the increasing repulsive forces between insulin molecules as the magnitude of the polypeptide net charge increases.

On this assumption, we can estimate the contribution of electrostatic effects to the dissociation of fibrils by considering a colloidal model where each monomer in the fibril experiences a repulsive electrostatic interaction with its nearest neighbors, modeled by a screened Coulomb potential as

$$U_{ch} = \frac{Q^2}{4\pi\varepsilon_0\varepsilon r_0}e^{-r_0/r_D}, \tag{1}$$

where r_D is the Debye length, r_0 is the effective separation of the protein molecules in the fibril, ε_0 is the permittivity of a vacuum, and ε is the dielectric constant of water. In agreement with independent studies of other amyloid systems (30–33), the existence of a dynamic equilibrium between the fibrillar and soluble states of insulin was demonstrated in experiments exploring the reversibility of the dissociation reaction (see Fig. S3 and Fig. S4). We consider this equilibrium according to classical linear polymerization theory as: $m + x_j \rightleftharpoons x_{j+1}$, where $[m] = [x_1]$ is the monomer concentration, $[x_j]$ the concentration of fibrils with polymerization number j, and $K = [x_{j+1}]/([x_j][m])$ is the equilibrium constant, which we assume here to be constant for all polymerization numbers j (34). Similarly to an approach used by Narimoto et al. (30), we can then compute the fraction of soluble protein as

$$
\begin{aligned}
f &= \frac{[m]}{[m_{\text{tot}}]}\\
&= \frac{2[m_{\text{tot}}]e^{-\beta[\Delta G_0 + U_{\text{ch}}(Q)]} + 1 - \sqrt{4[m_{\text{tot}}]e^{-\beta[\Delta G_0 + U_{\text{ch}}(Q)]} + 1}}{2m_{\text{tot}}^2\, e^{-2\beta[\Delta G_0 + U_{\text{ch}}(Q)]}},
\end{aligned}
\tag{2}
$$

where $[m_{\text{tot}}] = \sum_{j=1}^{\infty} j[x_j] = [m]/(1-K[m])^2$ is the total concentration of protein in both fibrillar and soluble form, and $\beta = (RT)^{-1}$ is the inverse temperature. We have expressed the equilibrium constant as $K = e^{-\beta[\Delta G_0 + U_{\text{ch}}(Q)]}$, where the free energy difference between the soluble

and fibrillar state $\Delta G_{\text{tot}} = \Delta G_0 + U_{\text{ch}}(Q)$ has been split into an electrostatic part $U_{ch}(Q)$ given by Eq. 1, and the free energy difference between a soluble insulin monomer and a monomer within a fibril in the absence of charge, ΔG_0.

A fit of Eq. 3 to the data in Fig. 2 B reveals that these simple considerations based on electrostatic effects, which are utilized extensively in colloidal science (35), can describe accurately the dissociation of highly charged fibrils at high pH values, where $Q \leq 0$. Furthermore, we can acquire an estimate for the fibril stability in the absence of charge, $\Delta G_0 = -39.4 \pm 1.3$ kJ/mol, as well as the only other free parameter, the average distance between charges in the fibril, calculated as $r_0 = 1.48$ nm using a Debye length of 2 nm. Previously, charge per residue (rather than net charge) has been shown to be an accurate order parameter for predicting conformations of intrinsically disordered proteins (36).

Because this study involves only one protein, it has not been possible to distinguish between these two parameters. We note, however, that the obtained value of r_0 using Q is consistent with the expected distance between monomers in the fibril of ($2 \times 0.78 =$) 1.56 nm, based on each monomer occupying two β-strands in the fibril structure (37) and an intersheet distance of 0.78 nm (37). The stability of the fibrils determined here is of the same order of magnitude as that measured for amyloid fibrils composed of β_2-microglobulin and the β-amyloid peptide (30,31), indicative that the key interactions that stabilize amyloid fibrils in general are largely sequence-independent in nature. The ability to model accurately the characteristics of amyloid fibrils shown here using a coarse-grained approach is consistent with findings from previous studies that show that the rate of fibril elongation correlates inversely with polypeptide net charge (38). Taken together, these observations demonstrate that both fibril assembly and stability are highly sensitive to the global physicochemical character of the polypeptide chain.

Thermodynamic stability of fibrils is reduced by partial disruption of β-sheet structure

Although fibril dissociation was below detectable limits at pH values <pH 8.0, inspection of the fibrils by TEM showed substantial changes in their morphology between pH 4.0 and pH 8.0 (Fig. 1, *right panels*). To ascertain whether or not this phenomenon is related to changes in the intrinsic molecular structure of the fibrils under these conditions, we examined the fibrils by FTIR spectroscopy. The amide I' region of the FTIR spectrum (1600–1700 cm^{-1}) arises predominantly from carbonyl-stretching vibrations within the peptide bonds, and as such is highly sensitive to the secondary structure present in the polypeptide chain (21). The amide I' band in the FTIR spectrum of insulin fibrils at pH* 1.6 is shown in Fig. 3 and demonstrates a dominant peak at 1627 cm^{-1}
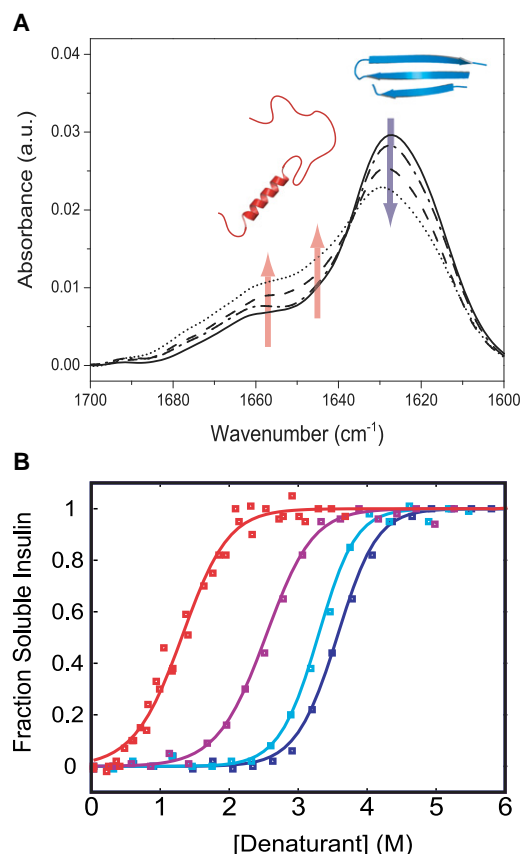
FIGURE 3 FTIR spectra and thermodynamic stability of insulin fibrils. (*A*) FTIR spectra of insulin fibrils formed at pH* 1.6 (*solid line*) and adjusted to pH* 3.6 (*dashed dotted line*), pH* 5.6 (*dashed line*), and pH* 7.6 (*dotted line*) by addition of NaOD. The secondary structure contributions determined from deconvolution of the spectra of the fibrils at pH* 1.6 and pH* 7.6 are given in the table panel in Fig. S1 in the Supporting Material. (*B*) Insulin fibrils were incubated in increasing concentrations of guanidinium thiocyanate at pH 2.0 (*dark blue squares*), pH 4.0 (*light blue squares*), pH 6.0 (*purple squares*), and pH 8.0 (*red squares*) for 48 h and the subsequent extent of dissociation determined. The data were fit to the linear polymerization model.

attributable to the presence of intermolecular β-sheet structure, a second major peak at 1657 cm^{-1} indicative of α-helix/turns/bends, and a small peak corresponding to random structure at 1645 cm^{-1} (21).

As the pH* of the fibril suspension is increased to pH* 3.6, only very small and subtle changes are observed in the spectrum; between pH* 3.6 and 7.6, however, a number of significant spectral changes are evident. The most pronounced is a decrease in the intensity of the peak at 1627 cm^{-1} with a concomitant increase in those at 1657 cm^{-1} and 1645 cm^{-1}, indicating a partial loss of ordered β-sheet structure. In addition, there is a subtle shift in the maximum of the β-sheet peak to higher frequencies indicative of an overall weakening of the hydrogen-bonding network in the fibril (39). Deconvolution of the spectra at pH* 1.6 and 7.6 was performed to estimate the secondary

structural content of the fibrils (see Fig. S1). These analyses indicate that the fibrils at pH* 1.6 contain 75% β-sheet structure, but that those at pH* 7.6 contain only 58% of such structure, indicating a relative decrease in β-sheet structure of 23%. This standard type of analysis assumes identical extinction coefficients for the different structural elements, and has been shown to be subject to absolute errors of 2.5–4% in structural content (21).

The behavior of the fibrils below pH 8.0 was further examined by comparing the resistance of the fibrils to dissolution by guanidinium thiocyanate (GdnSCN) (Fig. 3 *B*). Fibrils were incubated at between pH 2.0 and 8.0 in the presence of increasing concentrations of the denaturant for 48 h before ultracentrifugation. The fraction of insulin in the supernatant was again used as a measure of fibril dissociation. At pH 2.0, the fibrils appear to undergo a single dissociative transition with a midpoint of 3.75 M GdnSCN. As shown in Fig. 4 *A*, the fibrils at pH 4.0 are only slightly destabilized relative to those at pH 2.0; at pH 6.0 and 8.0, however, the fibrils are substantially destabilized, with dissociation midpoints of 2.5 M and 1.5 M GdnSCN, respectively. These data fit well to the linear polymerization model of Oosawa and Kasai (34), yielding fibril stabilities of $\Delta G = -56.3 \pm 1.2$, -55.4 ± 1.6, -43.2 ± 0.9, and -33.3 ± 0.6 kJ/mol at pH 2.0, 4.0, 6.0, and 8.0, respectively, where the quoted uncertainties correspond only to the error in fitting.

Hexameric insulin has previously been shown to be completely dissociated by 0.25 M GdnHCl (a weaker denaturant than GdnSCN) and insulin to be mostly monomeric at 2 M GdnHCl, even at pH 7.4 where oligomers are maximally stable, and a high concentration of 2 mg/ml (40). This justifies application of a model involving an equilibrium between monomeric and fibrillar insulin. In addition, similar *m*-values (related to the apparent slope) were obtained at each pH, ranging from 7.9 kJ/mol/M (pH 6) to 9.8 kJ/mol/M (pH 4), suggesting a similar change in solvent-accessible surface area in each case.

Remarkably, the stability of the fibrils determined here at pH 6.0, close to the predicted isoelectric point of the protein (5.5), is very similar to the fibril stability determined in the absence of charge by analysis of the effects of electrostatic interactions as detailed above (Fig. 2 *B*, $\Delta G_0 = -39.4 \pm 1.3$ kJ/mol). To explore the origin of the dramatic decrease in fibril stability between pH 2.0 and 8.0, the fibril stabilities were considered as a function of the relative intensities of the main β-sheet peak in the FTIR spectra (Fig. 4 *B*). The resulting correlation coefficient of $r_4 = -0.99$, $p < 0.01$, demonstrates that fibril stability is strongly related to the fraction of β-sheet structure within the fibrils, and therefore is strongly influenced by the interactions within the cross-β network.

Unlike the high pH regime, above pH 8.0, in which we observe fibril dissociation, the changes in fibril structure and stability between pH 2.0 and 8.0 cannot be modeled
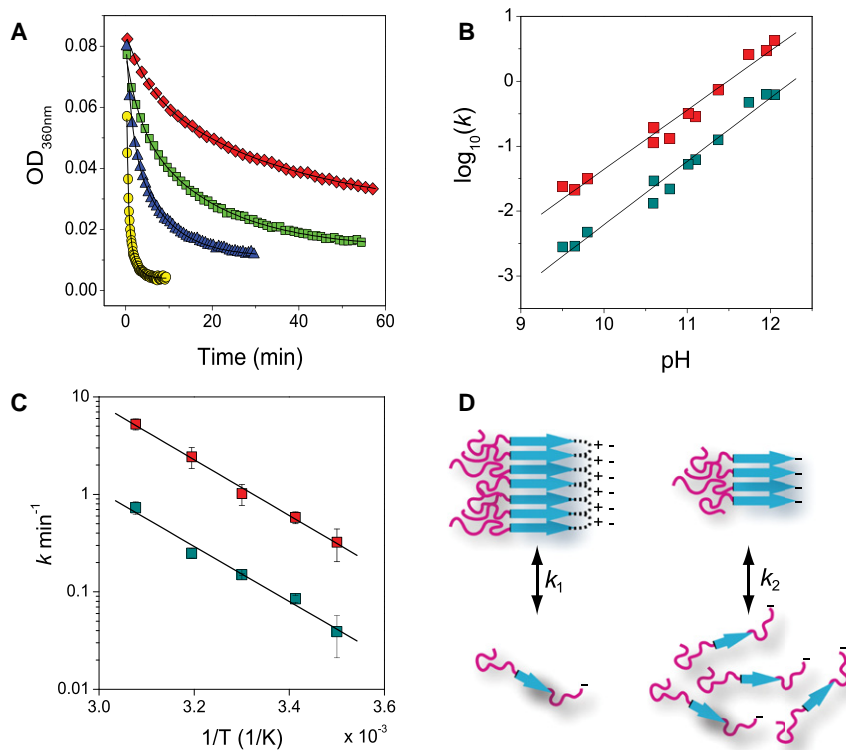
FIGURE 4 pH and temperature dependence of the kinetics of insulin fibril dissociation. (*A*) Insulin fibril dissociation kinetics were followed by turbidity. Representative kinetic traces are shown for insulin solutions adjusted to pH 10.6 (*red diamonds*), 11.0 (*green squares*), 11.4 (*blue triangles*), and 12.0 (*yellow circles*). The lines represent the double-exponential functions that best fit the data. (*B*) Dependence of the fitted rate constants on pH. (*C*) Dependence of the fitted rate constants for fibril dissociation at pH 11.3 on inverse temperature in the range 15–50°C. These data represent the average of three independent experiments. (*Solid lines*, panels *B* and *C*) Linear fits to the data. (*D*) The cartoon illustrates the strong influence of a single ionization event on the kinetics of fibril dissociation. (*Left*) When Arg-B22 forms a stabilizing intra- or interchain salt bridge with a negatively charged moiety, dissociation is a rare event (k_1). When this salt bridge is disrupted (*right*), the rate of dissociation increases dramatically (k_2).

in terms of simple charge repulsion, given that the net charge of the protein molecule changes from positive to negative in this pH range. Furthermore, between pH 2.0 and 8.0 the unfolding of a discrete proportion of β-sheet structure within the fibrils indicates that local rather than global changes may govern, at least in part, the changes observed in this pH range. In this case, the disruption of one or more ionic interactions in association with the increase in the pH from 2.0 to 8.0, could trigger a change in fibril structure that impacts on the stability of the fibrils. Based on the distribution of pK_a values for amino-acid side chains within the context of folded proteins (29), any of the four glutamic acid or two histidine side-chain moieties are capable of participating in an ionic interaction that could be disrupted in this pH range.

If, therefore, a glutamic acid or histidine side chain forms a salt bridge at pH 2.0 with a partially buried group of opposite charge, disruption of this interaction as the solution pH increases will result in a partial reorganization of the structure to solvate the resulting highly energetically unfavorable buried charge. Our observation from FTIR that the β-sheet content of the fibrils decreases from 75% (pH 2.0) to 57% (pH 8.0), indicates that between eight and nine hydrogen bonds within the total sequence length of 51 residues are disrupted to accommodate this structural reorganization. In support of this speculation, we note that the breakage of 8−9 hydrogen bonds with an energy of 2.1–6.3 kJ/mol per bond is similar in magnitude to the energetic penalty

for the burial of a charge in the interior or the protein structure (~21 kJ/mol (41)).

The kinetics of insulin fibril dissociation is dependent on the ionization state of a single side chain

After this analysis, we returned our attention to the pH range in which dissociation readily takes place by examining the kinetics of insulin fibril dissociation. Such dissociation was induced by the addition of sodium hydroxide and monitored by following the decrease in solution turbidity during the course of the reaction (Fig. 4 *A*). These kinetic data were then analyzed by fitting to a double-exponential function (see Materials and Methods). The two decay rates (k) differ by almost an order of magnitude and appear to be directly proportional to each other ($R = 0.99$) with a proportionality constant of 7.6 $\pm$ 0.2 (Fig. 4 *B*). An analysis of the temperature dependence of the two rate constants at pH 11.3 reveals that, within the temperature range 15–50°C, both of these processes are, to a very good approximation, governed by Arrhenius-type behavior (Fig. 4 *C*).

This observation does not exclude deviations from classical Arrhenius behavior—i.e., changing heat capacity, outside this temperature range, as is commonly seen in the case of protein folding over larger temperature ranges (42). Arrhenius-type behavior has previously been observed in amyloid formation (43,44). Based on these data, the

enthalpic activation barriers calculated for the fast and slow dissociation rates are 55 ± 2 kJ/mol and 54 ± 4 kJ/mol, respectively. The similarity of these two values strongly suggests that the fast and slow rate constants for the dissociation reaction monitor the same fundamental chemical event. These activation energies are, interestingly, similar in magnitude to, but smaller than, the activation energy for the reorganization of insulin molecules that occurs as they attach to the fibril ends under optimal conditions for growth at pH 2.0 where $\Delta H^{\ddagger}_{growth} = 102.5$ kJ/mol (44).

As shown in Fig. 4 B, the dissociation rates have a strong dependence on the final solution pH. A plot of log k against pH (Fig. 4 B) shows linear regions with gradients of 0.98 ± 0.05 for the slow phase and 0.91 ± 0.05 for the fast phase, indicating that both rates are approximately inversely proportional to the number of hydrogen ions free in solution. A comparison of the results with a modified mathematical model for rationalizing the pH dependence of protein denaturation (see the Supporting Material) shows that the gradient of close to unity suggests that the kinetics of insulin fibril dissociation are regulated by the charge state of a single amino-acid residue.

Further to this conclusion, the analysis stipulates that the pK_a of this residue must be higher than the pH range for which log k displays a linear dependence on pH, indicating that the pK_a of the amino acid must be above 12.0. This finding suggests a critical role under these highly destabilizing conditions for the unique arginine residue (pK_a 12.3) at position B22, whereby this residue may participate in a salt bridge capable of kinetically stabilizing the fibrils against rapid dissociation. The pK_a values of both lysine and tyrosine side chains, however, have been observed to exceed 12.0 within the folded context of some proteins, and as such we cannot rule out that one of the four tyrosine residues or the unique lysine residue in the sequence may account for our observations.

CONCLUSION

Many polypeptides and proteins with variable primary sequences can assemble into amyloid fibrils; different solution conditions, however, are often required to tune the chemical properties of the amino-acid side chains, such as their charge, to facilitate this conversion (45). We have demonstrated in this article that, even once formed, the stability of fibrillar species, typically highly resistant to dissociation, is susceptible to the pH-induced ionization of side-chain moieties. The stability of fibrils composed of the protein insulin prepared at pH 2.0 and then suspended in buffers of various pH, can be divided into three different pH regimes. Insulin fibrils are highly stable at low pH values (2.0–4.0). At pH values in the range 4.0–8.0, however, the disruption of specific electrostatic interactions results in structural reorganization and a decrease in size of the β-sheet network, with a concomitant decrease in the thermo-

dynamic stability of the fibrils. Above this pH range the increasingly negative net charge on the insulin molecules drives substantial dissociation of the fibrils as a result of increasing electrostatic repulsive forces.

Our data demonstrate in addition that specific interactions between side-chain groups, such as salt bridges, can influence the structure and stability of the fibrils in a rational manner. Within the context of globular proteins, ionic pairing interactions are capable of stabilizing native folds relative to the unfolded state both thermodynamically and kinetically (46–49). The data presented here show that specific electrostatic interactions may also play a similar role within the architecture of amyloid fibrils.

Globular proteins have a well-defined three-dimensional structure under their native conditions, encoded by their amino-acid sequence, which has been optimized (to varying extents) by evolution (50) to guarantee reliable folding. This structure is destabilized outside the relatively narrow working pH range of the protein. In contrast, amyloid fibrils may be formed from the same protein under a variety of conditions. For example, insulin may form amyloid fibrils both at acidic and at neutral pH values, resulting in structures that are morphologically distinct (51). Indeed, techniques such as AFM and cryo-EM have shown multiple strains of insulin amyloid fibrils to coexist within the same solution (37).

The persistence of the observed fibril types implies that they are likely to be some of the most thermodynamically stable structures under the conditions that promote their formation. In agreement with this idea, in this article we observed the fibrils to be maximally stable under their growth conditions. This suggests that these conditions favor the more specific stabilizing interactions such as salt bridges, which drive the assembly process, and subsequently contribute to the thermodynamic stability of the final structure. The electrostatic repulsion model discussed in this study is coarse-grained, involving no such specific interactions, and thus does not describe the behavior close to the fibril-forming conditions where specific interactions dominate. However, at high pH values where specific stabilizing interactions have been disrupted, we have found the soluble-fibril protein equilibrium to be well explained by principles commonly applied in the field of colloid science (35).

The correlation observed in this study between β-sheet content and fibril stability supports the idea (13) that the highly ordered (52) cross-β array of hydrogen bonds within amyloid fibrils represents an essential requirement for their very high stability. Remarkably, the energy required to unfold the native state of insulin molecules in solution (44) is fivefold lower than that required to dissociate insulin molecules from amyloid fibrils under identical conditions. This finding indicates that insulin is capable of making more stable intermolecular interactions than the intramolecular ones that stabilize its globular fold and suggests that the

fibrillar state can be thermodynamically more stable than the native state.

SUPPORTING MATERIAL

REFERENCES

1. Chiti, F., and C. M. Dobson. 2006. Protein misfolding, functional amyloid, and human disease. *Annu. Rev. Biochem.* 75:333–366.

2. Fowler, D. M., A. V. Koulov, …, J. W. Kelly. 2006. Functional amyloid formation within mammalian tissue. *PLoS Biol.* 4:e6.

3. Chapman, M. R., L. S. Robinson, …, S. J. Hultgren. 2002. Role of *Escherichia coli* curli operons in directing amyloid fiber formation. *Science.* 295:851–855.

4. Dobson, C. M. 2003. Protein folding and misfolding. *Nature.* 426:884–890.

5. Knowles, T. P., A. W. Fitzpatrick, …, M. E. Welland. 2007. Role of intermolecular forces in defining material properties of protein nanofibrils. *Science.* 318:1900–1903.

6. Sunde, M., L. C. Serpell, …, C. C. Blake. 1997. Common core structure of amyloid fibrils by synchrotron x-ray diffraction. *J. Mol. Biol.* 273:729–739.

7. Nelson, R., M. R. Sawaya, …, D. Eisenberg. 2005. Structure of the cross-β spine of amyloid-like fibrils. *Nature.* 435:773–778.

8. Gazit, E. 2002. The "correctly folded" state of proteins: is it a metastable state? *Angew. Chem. Int. Ed. Engl.* 41:257–259.

9. Meersman, F., and C. M. Dobson. 2006. Probing the pressure-temperature stability of amyloid fibrils provides new insights into their molecular properties. *Biochim. Biophys. Acta.* 1764:452–460.

10. Fowler, D. M., A. V. Koulov, …, J. W. Kelly. 2007. Functional amyloid—from bacteria to humans. *Trends Biochem. Sci.* 32:217–224.

11. Macphee, C. E., and D. Woolfson. 2004. Engineered and designed peptide-based fibrous biomaterials. *Curr. Opin. Solid St. Matter.* 8:141–149.

12. Makin, O. S., E. Atkins, …, L. C. Serpell. 2005. Molecular basis for amyloid fibril formation and stability. *Proc. Natl. Acad. Sci. USA.* 102:315–320.

13. Sawaya, M. R., S. Sambashivan, …, D. Eisenberg. 2007. Atomic structures of amyloid cross-β spines reveal varied steric zippers. *Nature.* 447:453–457.

14. Petkova, A. T., W.-M. Yau, and R. Tycko. 2006. Experimental constraints on quaternary structure in Alzheimer's β-amyloid fibrils. *Biochemistry.* 45:498–512.

15. Williams, A. D., S. Shivaprasad, and R. Wetzel. 2006. Alanine scanning mutagenesis of Aβ (1–40) amyloid fibril stability. *J. Mol. Biol.* 357:1283–1294.

16. Devlin, G. L., T. P. Knowles, …, C. E. MacPhee. 2006. The component polypeptide chains of bovine insulin nucleate or inhibit aggregation of the parent protein in a conformation-dependent manner. *J. Mol. Biol.* 360:497–509.

17. Du Vigneaud, V., R. Sifferd, and R. Sealock. 1933. The heat precipitation of insulin. *J. Biol. Chem.* 102:521–533.

18. Waugh, D. F. 1948. Regeneration of insulin from insulin fibrils by the action of alkali. *J. Am. Chem. Soc.* 70:1850–1857.

19. Krebs, M. R., C. E. Macphee, …, A. M. Donald. 2004. The formation of spherulites by amyloid fibrils of bovine insulin. *Proc. Natl. Acad. Sci. USA.* 101:14420–14424.

20. Nilsson, M. R., and C. M. Dobson. 2003. Chemical modification of insulin in amyloid fibrils. *Protein Sci.* 12:2637–2641.

21. Byler, D. M., and H. Susi. 1986. Examination of the secondary structure of proteins by deconvolved FTIR spectra. *Biopolymers.* 25:469–487.

22. Bradford, M. M. 1976. A rapid and sensitive method for the quantitation of microgram quantities of protein utilizing the principle of protein-dye binding. *Anal. Biochem.* 72:248–254.

23. Malisauskas, M., C. Weise, …, L. Morozova-Roche. 2010. Lability landscape and protease resistance of human insulin amyloid: a new insight into its molecular properties. *J. Mol. Biol.* 396:60–74.

24. Blundell, T., G. Dodson, …, D. Mercola. 1972. Insulin: the structure in the crystal and its reflection in chemistry and biology. *Adv. Protein Chem.* 26:279–402.

25. Fredericq, E. 1953. Reversible dissociation of insulin. *Nature.* 171:570–571.

26. Jeffrey, P. 1963. Apparent molecular weight of insulin in dilute acid solution. *Nature.* 197:1104–1105.

27. Jeffrey, P. D. 1974. Polymerization behavior of bovine zinc-insulin at neutral pH. Molecular weight of the subunit and the effect of glucose. *Biochemistry.* 13:4441–4447.

28. Milthorpe, B. K., L. W. Nichol, and P. D. Jeffrey. 1977. The polymerization pattern of zinc(II)-insulin at pH 7.0. *Biochim. Biophys. Acta.* 495:195–202.

29. Pace, C. N., G. R. Grimsley, and J. M. Scholtz. 2009. Protein ionizable groups: pK values and their contribution to protein stability and solubility. *J. Biol. Chem.* 284:13285–13289.

30. Narimoto, T., K. Sakurai, …, Y. Goto. 2004. Conformational stability of amyloid fibrils of β2-microglobulin probed by guanidine-hydrochloride-induced unfolding. *FEBS Lett.* 576:313–319.

31. Williams, A. D., E. Portelius, …, R. Wetzel. 2004. Mapping Aβ amyloid fibril secondary structure using scanning proline mutagenesis. *J. Mol. Biol.* 335:833–842.

32. O'Nuallain, B., S. Shivaprasad, …, R. Wetzel. 2005. Thermodynamics of A β (1–40) amyloid fibril elongation. *Biochemistry.* 44:12709–12718.

33. Carulla, N., G. L. Caddy, …, C. M. Dobson. 2005. Molecular recycling within amyloid fibrils. *Nature.* 436:554–558.

34. Oosawa, F., and M. Kasai. 1962. A theory of linear and helical aggregations of macromolecules. *J. Mol. Biol.* 4:10–21.

35. Pashley, R., and M. Karaman. 2004. Applied Colloid and Surface Chemistry. John Wiley & Sons, New York.

36. Mao, A. H., S. L. Crick, …, R. V. Pappu. 2010. Net charge per residue modulates conformational ensembles of intrinsically disordered proteins. *Proc. Natl. Acad. Sci. USA.* 107:8183–8188.

37. Jiménez, J. L., E. J. Nettleton, …, H. R. Saibil. 2002. The protofilament structure of insulin amyloid fibrils. *Proc. Natl. Acad. Sci. USA.* 99:9196–9201.

38. Chiti, F., M. Stefani, …, C. M. Dobson. 2003. Rationalization of the effects of mutations on peptide and protein aggregation rates. *Nature.* 424:805–808.

39. Nilsson, M. R. 2004. Techniques to study amyloid fibril formation in vitro. *Methods.* 34:151–160.

40. Ahmad, A., I. S. Millett, …, A. L. Fink. 2003. Partially folded intermediates in insulin fibrillation. *Biochemistry.* 42:11404–11416.

41. Fersht, A. 1999. Structure and Mechanism in Protein Science. W.H. Freeman, New York.

42. Oliveberg, M., Y. J. Tan, and A. R. Fersht. 1995. Negative activation enthalpies in the kinetics of protein folding. *Proc. Natl. Acad. Sci. USA.* 92:8926–8929.

43. Kusumoto, Y., A. Lomakin, ..., G. B. Benedek. 1998. Temperature dependence of amyloid β-protein fibrilization. *Proc. Natl. Acad. Sci. USA.* 95:12277–12282.

44. Knowles, T. P. J., W. Shu, ..., M. E. Welland. 2007. Kinetics and thermodynamics of amyloid formation from direct measurements of fluctuations in fibril mass. *Proc. Natl. Acad. Sci. USA.* 104:10016–10021.

45. DuBay, K. F., A. P. Pawar, ..., M. Vendruscolo. 2004. Prediction of the absolute aggregation rates of amyloidogenic polypeptide chains. *J. Mol. Biol.* 341:1317–1326.

46. Oliveberg, M., and A. R. Fersht. 1996. New approach to the study of transient protein conformations: the formation of a semiburied salt link in the folding pathway of barnase. *Biochemistry.* 35:6795–6805.

47. Kumar, S., and R. Nussinov. 1999. Salt bridge stability in monomeric proteins. *J. Mol. Biol.* 293:1241–1255.

48. Bosshard, H. R., D. N. Marti, and I. Jelesarov. 2004. Protein stabilization by salt bridges: concepts, experimental approaches and clarification of some misunderstandings. *J. Mol. Recognit.* 17:1–16.

49. Zubillaga, R. A., E. García-Hernández, ..., J. Polaina. 2006. Effect of a new ionic pair on the unfolding activation barrier of β-glucosidase B. *Protein Pept. Lett.* 13:113–118.

50. Zeldovich, K. B., and E. I. Shakhnovich. 2008. Understanding protein evolution: from protein physics to Darwinian selection. *Annu. Rev. Phys. Chem.* 59:105–127.

51. Hong, D. P., and A. L. Fink. 2005. Independent heterologous fibrillation of insulin and its β-chain peptide. *Biochemistry.* 44:16701–16709.

52. Knowles, T. P. J., J. F. Smith, ..., M. E. Welland. 2006. Spatial persistence of angular correlations in amyloid fibrils. *Phys. Rev. Lett.* 96:238301.